energies

MDPI

Article

Parameter Estimation Method for Virtual Power Plant Frequency Response Model Based on SLP

Zheng Shi [1,*], Haixiao Zhu [2], Haibo Zhao [1], Peng Wang [1], Yan Liang [1,3], Kaikai Wang [1], Jie Chen [1], Xiaoming Zheng [1] and Hongli Liu [1]

[1] Economic and Technical Research Institute of State Grid Shanxi Electric Power Company, Taiyuan 030000, China; zhb8711@163.com (H.Z.); wangpeng@163.com (P.W.); liangyan_lyly@163.com (Y.L.); wangkaikai510@163.com (K.W.); serenachen@126.com (J.C.); ysuzhxm@126.com (X.Z.); liuhonglifriend@126.com (H.L.)

[2] School of Electrical and Power Engineering, Taiyuan University of Technology, Taiyuan 030024, China; 2023510359@link.tyut.edu.cn

[3] School of Electrical and Electronic Engineering, North China Electric Power University, Beijing 100000, China

* Correspondence: shizheng_sgcc@163.com; Tel.: +86-1326-161-1011

Abstract: In adapting to the double-high development trend of high-voltage direct current (HVDC) receiving-end power systems and solving optimization problems in emergency frequency control (EFC) supporting virtual power plants (VPPs) in large-scale power systems, a parameter estimation method for a VPP frequency response model based on a successive linear programming (SLP) method is proposed. First, a "centralized/decentralized" hierarchical control architecture for VPP participation in EFC is designed. Second, the frequency response characteristics of multiple flexible resources are scientifically analyzed, and the system frequency response (SFR) model and equivalent model of VPP are constructed. Subsequently, parameter estimation of the VPP frequency response model is carried out based on the SLP method, aiming to balance the accuracy and computational efficiency of the model. Finally, the effectiveness of the proposed methodology is verified by using PSD-BPA to simulate and test the three-zone HVDC recipient area grid.

Keywords: virtual power plant; emergency frequency control; system frequency response model; parameter estimation

check for updates

Citation: Shi, Z.; Zhu, H.; Zhao, H.; Wang, P.; Liang, Y.; Wang, K.; Chen, J.; Zheng, X.; Liu, H. Parameter Estimation Method for Virtual Power Plant Frequency Response Model Based on SLP. *Energies* **2024**, *17*, 3124. https://doi.org/10.3390/en17133124

Academic Editor: Ahmed Abu-Siada

Received: 18 May 2024
Revised: 15 June 2024
Accepted: 21 June 2024
Published: 25 June 2024
Corrected: 23 September 2024

Copyright: © 2024 by the authors. Licensee MDPI, Basel, Switzerland. This article is an open access article distributed under the terms and conditions of the Creative Commons Attribution (CC BY) license (https://creativecommons.org/licenses/by/4.0/).

1. Introduction

In the process of building a new power system in China, the rapid growth of installed capacity and the power generation of inverter interface power sources, such as wind power, energy storage, HVDC, etc., has brought to the fore the issue of grid frequency security [1,2]. As a potential frequency modulation resource, the virtual power plant (VPP) [3–5] can aggregate a wide range of types of flexible resources to holistically participate in grid regulation and assist the large grid in emergency frequency control [6,7]. Therefore, it is extremely important to construct a reasonable VPP frequency response model to accurately and quickly reflect its frequency response characteristics and regulation capability.

Accurate modeling of the VPP is the basis and prerequisite for its participation in the scheduling and control of large power grids. Reference [8] proposes a multi-timescale responsiveness assessment model for VPP with EVs as the main resource based on the responsiveness model of a single EV. Reference [9] considers the uncertainty impact of a wind power grid connection and V2G, and establishes a double-layer inverse robust optimization scheduling model with VPP. Reference [10] establishes an extended SFR model that takes into account the transient frequency modulation process of the VPP, which leads to a new thought for the overall participation of the VPP in frequency control but does not consider the way of controlling each resource within the VPP. Reference [11] treats wind turbines, energy storage devices, and motor loads as frequency modulation resources in the

VPP and constructs a primary frequency modulation model for the VPP to participate in the frequency control of the power system, but the study lacks a description of the overall frequency control characteristics of the VPP. Reference [12] proposes an SFR model based on inverter droop control for various types of distributed resources, but the model has a uniform and simple model structure, which makes it difficult to accurately reflect the control characteristics of each flexible resource.

Existing research related to VPP is mostly related to the power market, economic dispatch, and other fields [13,14], which are slightly insufficient in the optimization of parameter estimation for VPP frequency response models. Reference [15] presents a VPP model for transient stability analysis with VPP resources for current source and voltage source inverters. Reference [16] develops an equivalent aggregation model based on VPP frequency effects, which mainly considers different response delays among different distributed resources. In terms of parameter estimation, Reference [17] comes up with a way to estimate the equivalent inertia of a system based on polynomial fitting of frequency curves. Reference [18] raises a method for estimating the equivalent inertia and damping coefficients of synchronous and nonsynchronous power supplies based on closed-loop control. Reference [19] utilizes section information to estimate the equivalent frequency response model parameters of interconnected multi-area systems.

In summary, the following difficulties arise in modeling the frequency response characteristics of VPP. (1) VPP brings together many heterogeneous and flexible resources, and each resource participates in frequency modulation with different control modes and response characteristics. Therefore, how to collaborate various resources and construct a VPP frequency response model accurately reflecting the characteristics of the multi-flexible resources to support the emergency frequency control of the power system needs to be studied. (2) The VPP frequency response model is complex and of high-order and has many control parameters; the detailed model can ensure the calculation accuracy but also limit the decision-making efficiency of emergency frequency control; and the VPP model parameters are time-varying, which are different under different operating conditions of the grid, which exacerbates the complexity of the decision making of emergency frequency control taking into account the VPP. How to obtain model parameter estimations that take into account both accuracy and computational efficiency is still an open problem.

To overcome the problems mentioned above, this paper first comes up with a VPP hierarchical control architecture suitable for emergency frequency control. Secondly, the detailed frequency response model of VPP is constructed based on the response characteristics of multiple flexible resources. Then, the complex feedback control branch is aggregated to obtain its equivalent model, and the parameter estimation model is constructed and solved based on successive linear programming (SLP). Finally, the scientific validity of the proposed method is confirmed by multi-fault scenario testing based on a three-region HVDC receiving area grid.

2. Hierarchical Control Architecture of VPPs for Emergency Frequency Control

In this paper, we present a centralized/decentralized hierarchical architecture for emergency frequency control of VPPs, as shown in Figure 1. The architecture consists of three control layers: the centralized control layer, the VPP aggregation layer, and the local control layer.

The main body of the central control layer includes the grid control core and the VPP control master. The control core issues specific power control command values $\sum_i^{N_V} P_{eov_q}$, a system minimum frequency threshold f_{nadir}^{eo}, and a quasi-steady-state frequency threshold f_{qss}^{eo} according to the power deficit and frequency response capability of VPP, and monitors the grid frequency deviation in real time. The VPP control master reports in real-time the maximum support power $\sum_i^{N_V} P_{arv_m}$ that all VPPs in the network can provide, the steady-state support power $\sum_i^{N_V} P_{arv_q}$, the minimum value of the system frequency f_{nadir}^{ar}, and the quasi-steady-state frequency(QSSF) f_{qss}^{ar} after the VPPs join the process of emergency frequency control according to the given power command in case of a foreseen failure.

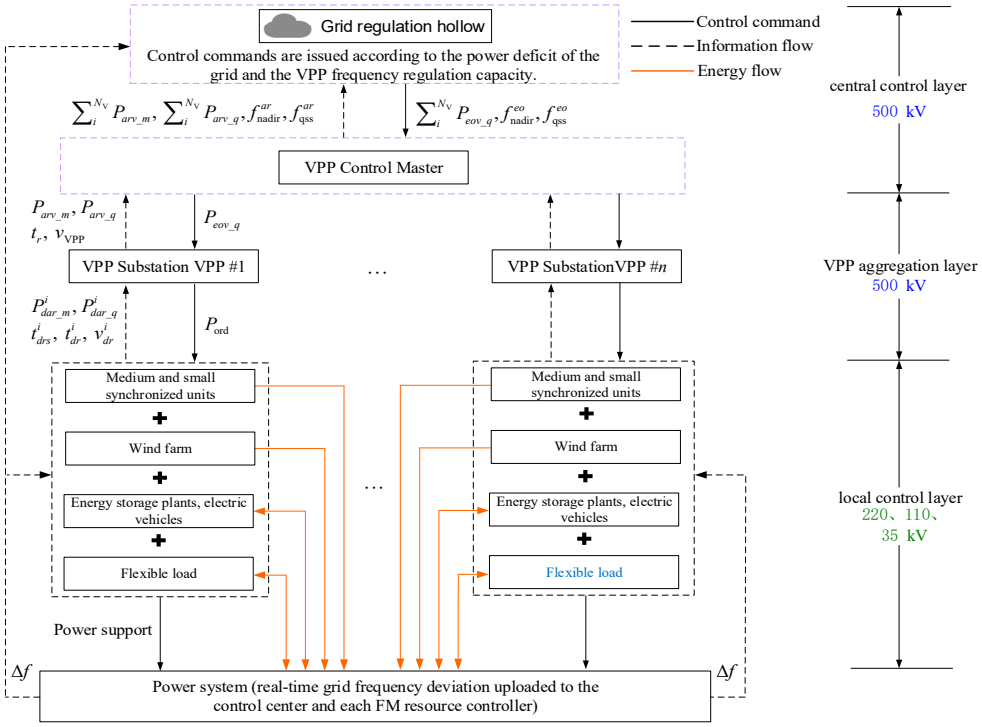


Figure 1. "Centralized/decentralized" VPP hierarchical control framework.

The main body of the VPP aggregation layer is the VPP sub-station under each 500 kV bus. The VPP sub-station receives, on the one hand, the maximum support power $P^i_{dar_m}$, the steady state power $P^i_{dar_q}$, the control response time t^i_{drs}, the power climbing time t^i_{dr}, and the climbing rate v^i_{dr} that each control resource can provide and, accordingly, reports the maximum regulation power P_{arv_m}, the steady-state regulation power P_{arv_q}, the climbing time t_r, and the climbing rate v_{vpp} that this sub-station can provide. On the other hand, according to the power support quantity P_{eov_q} issued by the VPP master station and the operation status of each control resource in the sub-station, the VPP sub-station co-ordinates and allocates the power command value P_{ord} to the multiple types of flexible control resources in the station.

The subjects in the local control layer include small- and medium-sized turbine units, distributed wind turbines, energy storage power stations, cluster electric vehicles, and flexible loads. When an active deficit fault occurs in the HVDC recipient area grid, as control terminals, each control resource will participate in emergency frequency control, provide power support, and safeguard grid frequency security. It should be noted that there are differences in the control characteristics of the resources, which have different forms of power support.

This architecture mainly includes three control levels: central control layer, VPP aggregation layer, and local control layer. In terms of communication, the communication between the power grid control center and the control master station, the control master station and sub-stations, and the control sub-stations and various distributed resources is bidirectional. In terms of data, the power grid control center and the control master station implement the issuance of specific control instructions and monitoring of system frequency. On the one hand, the control sub-station can receive data provided by various control resources; on the other hand, it allocates instructions to flexible control resources within the station based on the power support issued by the control master station and the status of the control sub-station. In terms of control strategy, the control strategy is issued from the control center to the control master station, from the control master station to the control sub-station, and from the control sub-station to the local control layer. When there is an active power shortage fault in the HVDC receiving-end power system, as the control

terminal, each control resource will participate in emergency frequency control, provide power support, and ensure system frequency security.

3. Modeling the Frequency Response Characteristics of a VPP

3.1. Frequency Characteristic Modeling of Multiple Flexible Resources

Units with voltage levels of 220 kV and below include coal-fired units, gas-fired units, and mixed-use power plants (e.g., waste power plants, steel power plants, and paper power plants). The medium-sized unit speed control system connected to 220 kV can be modeled by the GS-TA model, and the small-sized unit speed control system connected to 110 kV and 35 kV can be modeled by the IEEEG2 model [20–22]. Distributed wind turbines can be involved in frequency modulation based on rotor kinetic control, the control architecture diagram of which is shown in Figure 2, where H_W is the virtual inertia time constant provided by the turbine, K_W is the tuning coefficient of the turbine, and T_w is the turbine control response time constant.

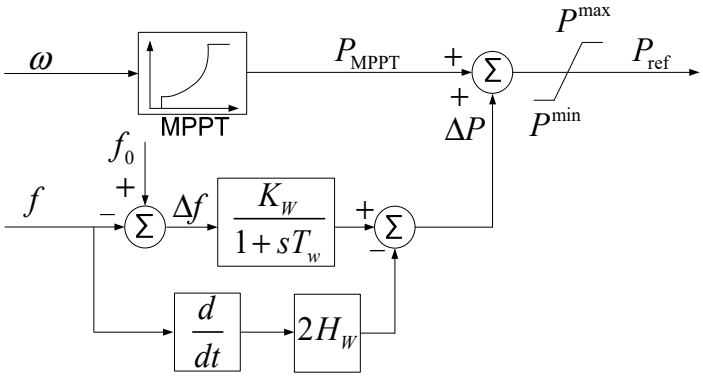


Figure 2. Diagram of WF active power reference control loop with the frequency regulation ability.

The energy storage plant can participate in frequency modulation based on fast power control with the power control function shown in Equation (1):

$$P_{\mathrm{ES}} = P_{\mathrm{ES}}^{\mathrm{ord}}[1 - (1 + \frac{T_{\mathrm{ES}}}{T_e})\mathrm{e}^{-\frac{t}{T_e}}] \tag{1}$$

In the above equation, $P_{\mathrm{ES}}^{\mathrm{ord}}$ and P_{ES} are the power command value and the actual output power value of the ESS issued by the VPP, and T_{ES} and T_e are the communication delay time and the control response time constant of the ESS from the occurrence of the fault to the control response.

The EV cluster can be equated to an energy storage power station, and the reverse charging is realized by the EV–grid interaction technology (vehicle to grid, V2G), whose power control function is shown in Equation (2):

$$P_{\mathrm{EV}} = P_{\mathrm{EV}}^{\mathrm{ord}}[1 - (1 + \frac{T_{\mathrm{EV}}}{T_{\mathrm{ev}}})\mathrm{e}^{-\frac{t}{T_{\mathrm{ev}}}}] \tag{2}$$

In the above equation, $P_{\mathrm{EV}}^{\mathrm{ord}}$ and P_{EV} are the power command value and the actual output power value of the EV issued by the VPP. T_{EV} and T_{ev} are the communication delay time and the control response time constant of the EV from the occurrence of the fault to the control response.

The way flexible loads (FLs) participate in frequency control is mainly divided into open-disconnected mode and regulation mode. Among them, the model of an open-break FL participating in frequency control is shown in Equation (3):

$$P_{\mathrm{FL},S} = P_{\mathrm{FL},S}^{\mathrm{ord}}[(t - T_{\mathrm{FL},S})] \tag{3}$$

In the above equation, $P_{FL,S}^{ord}$ and $P_{FL,S}$ are the control command value and the actual load-shedding amount of the open-break FL. $T_{FL,S}$ is the time interval between the occurrence of the fault and the load-shedding action of the open-break FL.

Based on Reference [23], the frequency response model of the modulated FL in one frequency modulation time scale is shown in Figure 3.

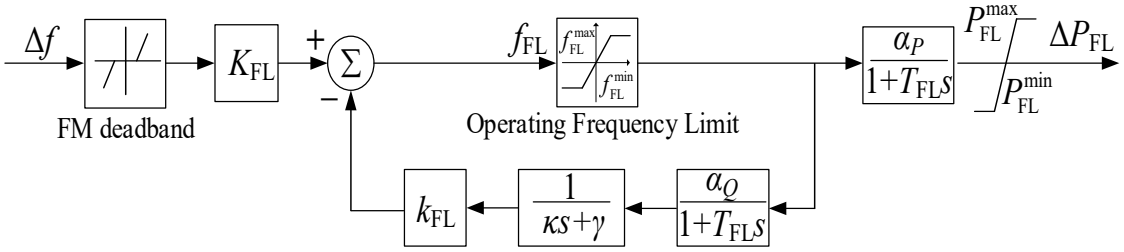


Figure 3. Frequency response model of adjustable FL.

In this model, K_{FL} is the tuning coefficient, Δf is the system frequency deviation, k_{FL} and T_{FL} denote the tuning coefficient and inertia time constant of the compressor controller, κ and γ are the equivalent thermodynamic parameters, α_P is the constant coefficient of electric power for normal operation of the FL, α_Q is the constant coefficient of refrigeration/heat of the FL, f_{FL} is the operating frequency of the FL, and f_{FL}^{max} and f_{FL}^{min} denote the upper and lower bounds of the operating frequency of the FL, respectively. P_{FL}^{max} and P_{FL}^{min} are the maximum and minimum limits of FL power. ΔP_{FL} is the amount of the power change of the FL.

3.2. VPP Frequency Response Modeling

Considering the frequency control characteristics of each flexible resource, the VPP frequency response model is shown in Figure 4:

$$\begin{cases} H_{VPP} = \sum_{i=1}^{N_G} H_{Gi}(S_{Gi}/S_{sys}) + \sum_{i=1}^{N_{WF}} H_{Wi}(S_{Wi}/S_{sys}) \\ D_{VPP} = \sum_{i=1}^{N_G} D_{Gi}(S_{Gi}/S_{sys}) + \sum_{i=1}^{N_{WF}} D_{Wi}(S_{Wi}/S_{sys}) \end{cases} \quad (4)$$

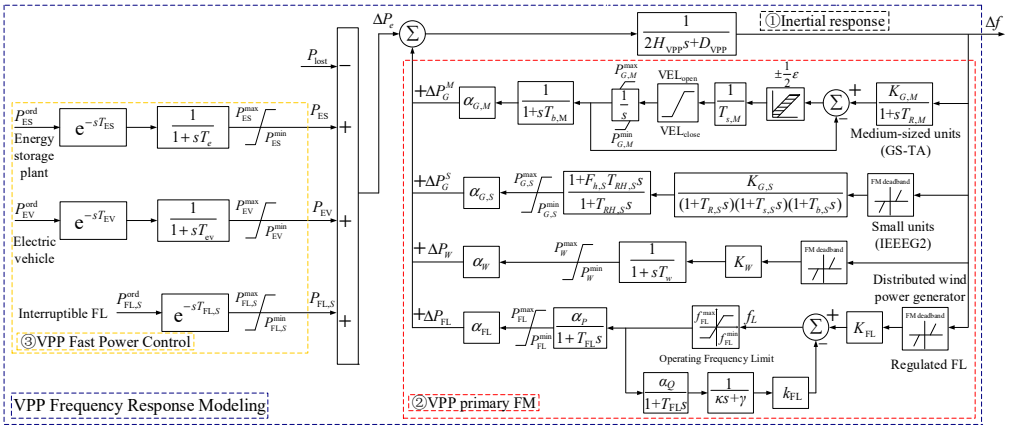


Figure 4. Frequency response model of VPP.

In the above equation, H_{VPP} is the equivalent inertia time constant provided by the VPP, H_{Gi} is the inertia time constant of the ith turbine unit, and NG is the number of units in the VPP in grid-connected operation, including small- and medium-sized units. H_{Wi} is the virtual inertia time constant provided by the ith wind turbine, and NWF is the number of wind turbines. S_{Gi}, and S_{Wi} are the rated powers of the ith turbine unit and wind turbine, respectively, and S_{sys} is the total installed system capacity. DVPP is the equivalent damping

coefficient of the system, and D_{Gi} is the damping factor of the ith turbine unit. D_{Wi} is the virtual damping factor provided by the ith wind turbine.

(1) Primary frequency modulation. The primary frequency modulation parameters for turbine units, distributed fans, and regulated FLs are as follows:

$$\begin{cases} K_{G,M} = \sum_{i=1}^{N_{\mathrm{MG}}} \alpha_{G,Mi} K_{G,Mi},\ K_{G,S} = \sum_{i=1}^{N_{\mathrm{SG}}} \alpha_{G,Si} K_{G,Si} \\ K_W = \sum_{i=1}^{N_{\mathrm{WF}}} \alpha_{Wi} K_{Wi},\ K_{\mathrm{FL}} = \sum_{i=1}^{N_{\mathrm{FL}}} \alpha_{\mathrm{FL}i} K_{\mathrm{FL}i} \end{cases} \tag{5}$$

In the above equation, $K_{G,M}$, $K_{G,S}$, K_W, and K_{FL} are the modulation coefficients for medium and small units, turbines, and regulated FLs. α is a constant coefficient representing the ratio of the rated power of the ith feedback control branch resource to the total capacity of that resource, and N_{MG}, N_{SG}, N_{WF}, and N_{FL} stand for the number of medium and small turbine units, turbines, and regulated FLs.

$$\begin{cases} X_{\mathrm{MG}} = \sum_{i=1}^{N_{\mathrm{MG}}} \lambda_i X_{\mathrm{MG}i}, X_{\mathrm{MG}} = \left\{ T_{b,M}, T_{s,M}, T_{R,M} \right\} \\ X_{\mathrm{SG}} = \sum_{i=1}^{N_{\mathrm{SG}}} \lambda_i X_{\mathrm{SG}i}, X_{\mathrm{SG}} = \left\{ T_{b,S}, T_{s,S}, T_{R,S}, T_{RH,S}, F_{h,S} \right\} \\ T_w = \sum_{i=1}^{N_{\mathrm{WF}}} \lambda_i T_{wi} \\ X_{\mathrm{FL}} = \sum_{i=1}^{N_{\mathrm{FL}}} \lambda_i X_{\mathrm{FL}i}, X_{\mathrm{FL}} = \left\{ T_{\mathrm{FL}}, \alpha_P, \alpha_Q, k_{\mathrm{SL}} \right\} \end{cases} \tag{6}$$

In the above equation, X_{MG}, X_{SG}, and X_{FL} represent the feedback control branch parameter sets of medium- and small-sized units and regulated FLs. $T_{b,M}$, $T_{s,M}$, and $T_{R,M}$ are the steam volume time constant, servo time constant, and governor response time constant for medium-sized units. $T_{b,S}$, $T_{s,S}$, $T_{R,S}$, $T_{RH,S}$, and $F_{h,S}$ are the steam volume time constant, servo time constant, governor response time constant, reheater time constant, and high-pressure cylinder power share for small-sized units, respectively. T_w is the response time constant for the turbine control and λ_i is the weighting coefficient of the ith feedback control branch.

(2) Fast power control. The control parameters of ESS, EV, and on-off FL are as follows:

$$\begin{cases} T_{\mathrm{ES}} = \sum_{i=1}^{N_{\mathrm{ES}}} \frac{P_{\mathrm{ES}i}}{P_{\mathrm{ES}}} T_{\mathrm{ES}i}\ , T_e = \sum_{i=1}^{N_{\mathrm{ES}}} \frac{P_{\mathrm{ES}i}}{P_{\mathrm{ES}}} T_{ei} \\ T_{\mathrm{EV}} = \sum_{i=1}^{N_{\mathrm{EV}}} \frac{P_{\mathrm{EV}i}}{P_{\mathrm{EV}}} T_{\mathrm{EV}i}\ , T_{ev} = \sum_{i=1}^{N_{\mathrm{EV}}} \frac{P_{\mathrm{EV}i}}{P_{\mathrm{EV}}} T_{evi} \\ T_{\mathrm{FL},S} = \sum_{i=1}^{N_{\mathrm{L}}} \frac{P_{\mathrm{FL},Si}}{P_{\mathrm{FL},S}} T_{\mathrm{FL},Si} \end{cases} \tag{7}$$

In the above equation, $P_{\mathrm{ES}i}$, $P_{\mathrm{Ev}i}$, and $P_{FL,Si}$ represent the actual output power of the *i*th branch of ESS, EV, and open FL. N_{ES}, N_{EV}, and N_{L} are the number of ESS, EV, and open FL.

4. SLP-Based Parameter Estimation Method for Frequency Response Model of VPP

4.1. Equivalent Methods for Frequency Response Modeling of VPPs

Since the VPP aggregates multiple types of heterogeneous resources, its feedback control branch is characterized by complex high-order and many parameters. The detailed model of frequency response taking into account multiple types of flexible resources has high accuracy, but it puts high requirements on simulation efficiency and model parameter estimation; at the same time, it is difficult to integrate in emergency frequency control optimization decisions. Aiming at the above difficulties, this section aggregates its complex feedback control branches to obtain the VPP frequency response equivalent model.

In the VPP frequency response model, the sum of each feedback control branch is a higher order transfer function. Therefore, the generalized transfer function $G_{\mathrm{VPP}}(s)$ is used to describe the VPP equivalent feedback control branch model in the general form:

$$G_{\mathrm{VPP}}(s) = \frac{b_m s^m + b_{m-1} s^{m-1} + \cdots + b_0}{a_n s^n + a_{n-1} s^{n-1} + \cdots + a_0}, \quad n \geq m \tag{8}$$

In the above equation, a_i, and b_j are the coefficients of the denominator and numerator polynomials, respectively. When the model order is one, its transfer function has an equivalent relationship with the simplified turbine governor model.

4.2. Parameter Estimation Optimization Model

For the SFR model after equating the VPP feedback control branch, the optimization model for VPP parameter estimation is established to minimize the frequency minimum point difference $\Delta f_{\mathrm{nadir},k}$ and QSSF difference $\Delta f_{\mathrm{qss},k}$ calculated from the detailed SFR model and the equating model under multiple types of foreseen fault scenarios, where Equation (9) is the objective function, and Equations (10) and (11) represent the system frequency nadir difference constraint and QSSF difference constraint, respectively. To avoid the frequency estimation value being higher than the true value of frequency, which causes the system leakage in the emergency frequency control optimization decision, the difference between the true value of the frequency index and the estimated value is set to be greater than zero. Equations (12) and (13) represent the limit constraints of each parameter in the estimation model.

$$\min \sum_{k=1}^{N_{\mathrm{K}}} \left(\Delta f_{\mathrm{nadir},k} + \Delta f_{\mathrm{qss},k} \right) \tag{9}$$

$$f_{\mathrm{nadir},k} - \hat{f}_{\mathrm{nadir},k}(a_i, b_j) \geq 0, \quad \forall i \in N_a, \quad \forall j \in N_b \tag{10}$$

$$f_{\mathrm{qss},k} - \hat{f}_{\mathrm{qss},k}(a_i, b_j) \geq 0, \quad \forall i \in N_a, \quad \forall j \in N_b \tag{11}$$

$$a_i^{\min} \leq a_i \leq a_i^{\max}, \forall i \in N_a \tag{12}$$

$$b_j^{\min} \leq b_j \leq b_j^{\max}, \forall j \in N_b \tag{13}$$

In the above equation, (9) is the objective function of parameter estimation, and NK represents the number of expected fault scenarios. $f_{\mathrm{nadir},k}$ and $\hat{f}_{\mathrm{nadir},k}$ are the minimum values of system frequency calculated by the detailed frequency response model and the equivalent model, respectively. N_a, and N_b are the numbers of parameters in the denominator and numerator of the equivalent model, respectively. $f_{\mathrm{qss},k}$ and $\hat{f}_{\mathrm{qss},k}$ are the quasi-steady-state frequencies obtained by the detailed frequency response model and the equivalent model, respectively. $a_i^{\max}$, $a_i^{\min}$, $b_i^{\max}$, and $b_i^{\min}$ are the upper and lower bounds of the parameters of the equivalent model, respectively.

The SFR is affected by various factors such as grid operation state, feedback control branch parameters, power deficit, etc., and its frequency dynamics are complex and nonlinear, which leads to the parameter estimation problem that VPP is not suitable to be solved directly. Therefore, the frequency difference constraints in Equations (10) and (11) are linearized based on the trajectory sensitivity method to establish the coupling relationship between the model parameters and the minimum and quasi-steady-state frequencies. The above optimization model can be rewritten as the following linear programming model:

$$\begin{aligned} \min \sum_{k=1}^{N_{\mathrm{K}}} \Big\{ & \left[f_{\mathrm{nadir},k} - \hat{f}_{\mathrm{nadir},k}(a_i, b_j) \right] \\ & + \left[f_{\mathrm{qss},k} - \hat{f}_{\mathrm{qss},k}(a_i, b_j) \right] \Big\} \end{aligned} \tag{14}$$

$$\begin{aligned}&\sum_{i=0}^{N_a}(\beta^k_{\text{nadir},i}\Delta a_i)+\sum_{j=0}^{N_b}(\beta^k_{\text{nadir},j}\Delta b_j)\\&\le f_{\text{nadir},k}-\hat{f}_{\text{nadir},k}(a_i^0,b_j^0),\\&\forall i\in N_a,\forall j\in N_b,\forall k\in N_K\end{aligned}\tag{15}$$

$$\begin{aligned}&\sum_{i=0}^{N_a}(\beta^k_{\text{qss},i}\Delta a_i)+\sum_{j=0}^{N_b}(\beta^k_{\text{qss},j}\Delta b_j)\\&\le f_{\text{qss},k}-\hat{f}_{\text{qss},k}(a_i^0,b_j^0),\\&\forall i\in N_a,\forall j\in N_b,\forall k\in N_K\end{aligned}\tag{16}$$

$$-a_i^0\le\Delta a_i\le a_i^{\max}-a_i^0,\forall i\in N_a\tag{17}$$

$$-b_j^0\le\Delta b_j\le b_j^{\max}-b_j^0,\forall j\in N_b\tag{18}$$

In the above equation, $\hat{f}_{\text{nadir},k}(a_i^0,b_j^0)$ and $\hat{f}_{\text{qss},k}(a_i^0,b_j^0)$ are the lowest values of the system frequency and the quasi-steady-state frequency of the equivalent model at the initial parameter settings. Δa_i, Δb_j is the variation of the model parameters. $\beta^k_{\text{nadir},i}$, $\beta^k_{\text{nadir},j}$ and $\beta^k_{\text{qss},i}$, $\beta^k_{\text{qss},j}$ are the frequency nadir sensitivity coefficients and QSSF sensitivity coefficients of the model parameters, respectively, as shown in Equation (19):

$$\begin{cases}\beta^k_{\text{nadir/qss},i}=\frac{\hat{f}_{\text{nadir/qss},k}(a_i,b_j,\kappa_{ai})-\hat{f}_{\text{nadir/qss},k}(a_i,b_j)}{\kappa_{ai}}\\\beta^k_{\text{nadir/qss},j}=\frac{\hat{f}_{\text{nadir/qss},k}(a_i,b_j,\kappa_{bj})-\hat{f}_{\text{nadir/qss},k}(a_i,b_j)}{\kappa_{bj}}\end{cases}\tag{19}$$

In the above equation, κ_{ai}, and κ_{bj} are the uptakes of the model parameters a_i, b_j.

4.3. SLP-Based Solution Algorithm

SLP is a mathematical optimization method used to solve nonlinear programming problems. It gradually approaches the optimal solution by decomposing nonlinear problems into a series of linear problems. The advantage of the SLP algorithm is that it decomposes complex nonlinear problems into a series of relatively simple linear problems, making the algorithm easier to implement and solve. The above parameter estimation optimization model is solved based on the SLP algorithm. The computational flow is shown in Figure 5.

Step 1: Initialization parameters. Extract the operating state data of multiple types of frequency modulation resources in the power grid and set the initial values of the equivalence model parameters a_i, $b_{j,}$ and the model order. Set the number of expected fault scenarios N_{K}, calculate the minimum frequency $f_{\text{nadir},k}$, quasi-steady-state frequency $f_{\text{qss},k}$, and the minimum frequency $\hat{f}_{\text{nadir},k}(a_i^0,b_j^0)$ and quasi-steady-state frequency $\hat{f}_{\text{qss},k}(a_i^0,b_j^0)$ of the system under each fault scenario from the detailed frequency response model, and the minimum frequency and quasi-steady-state frequency of the system from the equivalence model at the given initial values. Set the time-domain simulation time and step size, and the number of iterations $n = 0$.

Step 2: Optimize the solution. Firstly, the frequency key index difference constraint is linearized, and the VPP parameter estimation problem is transformed into a linear programming model. Set the regimes of a_i and b_j as 0.1, and calculate the minimum frequency of the system at the nth iteration and the QSSF sensitivity coefficient a_i^n and b_j^n according to Equation (19). Then, solve the linear programming model (Equations (14)–(18)) to obtain the model parameter variations Δa_i^n, Δb_j^n, and update the estimates at the nth iteration $a_i^{n+1}=a_i^n+\Delta a_i^n$, $b_j^{n+1}=b_j^n+\Delta b_j^n$.

Step 3: Termination judgment and parameter output. Judge whether the change of model parameters under the nth iteration is less than the cutoff error ε_a, ε_b or whether the parameter values a_i^n, b_j^n are out of the parameter design range. If satisfied, the calculation is terminated and the parameter estimation results are output; otherwise, make $n = n + 1$ and return to Step 2.

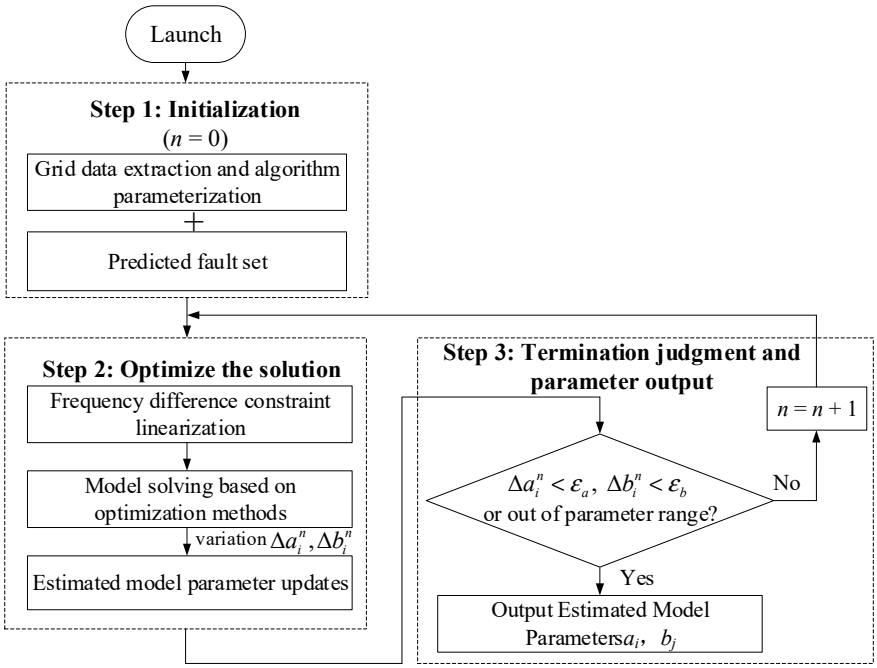


Figure 5. Parameter estimation process based on the SLP algorithm.

5. Simulation Analysis

5.1. Test Systems

This section is based on the electromechanical transient simulation software PSD-BPA (5.1.2) for verification. The test system is a three-region grid model (see Figure 6), and the VPP is configured in the HVDC receiving-end regional grid system C (see Figure 7); the main parameters are shown in Reference [24]. The test system is set up to access four large thermal power units at 500 kV, totaling 3.85 GW, and 18 VPPs, totaling 3.79 GW. In addition to the power fed by HVDC, the VPP capacity in the local grid region accounts for 49.6% of the generation resources. Taking VPP-1 as an example, the information on the types of resources and equipment capacities involved in frequency control within it is shown in Table 1.

Table 1. Frequency regulation resources in VPP-1.

Frequency Modulation Resources	Device Capacity/MW	Operating Power/MW	Control Method	Adjusted Power/MW	Trigger Method
gas turbine	54.0	42.0	inertia response and primary frequency modulation	12.0	response-driven
coal-fired unit	50.0	40.0	inertia response and primary frequency modulation	10.0	response-driven
wind power	22.5	22.5	rotor kinetic energy control	3.0	response-driven
energy storage plant	30.0	25.0	fast power control	5.0	event-triggering
electric vehicle	5.0	3.0	fast power control (V2G)	6.0	event-triggering
flexible load	5.0 (regulated)	3.0	one-time frequency modulation	3.0	response-driven
	3.0 (on-off)	2.0	load-shedding	2.0	event-triggering

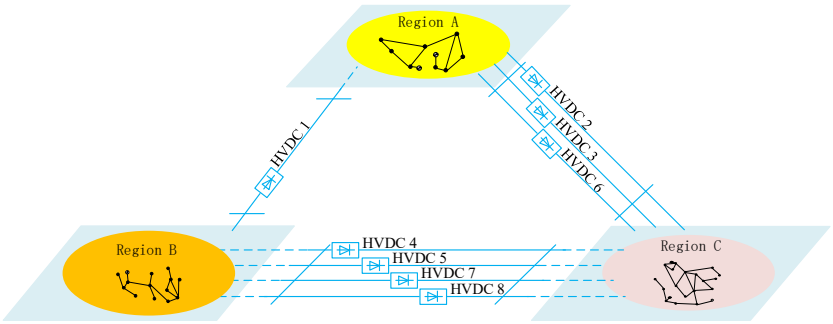


Figure 6. Schematic diagram of the HVDC interconnected power grid model with three regions.

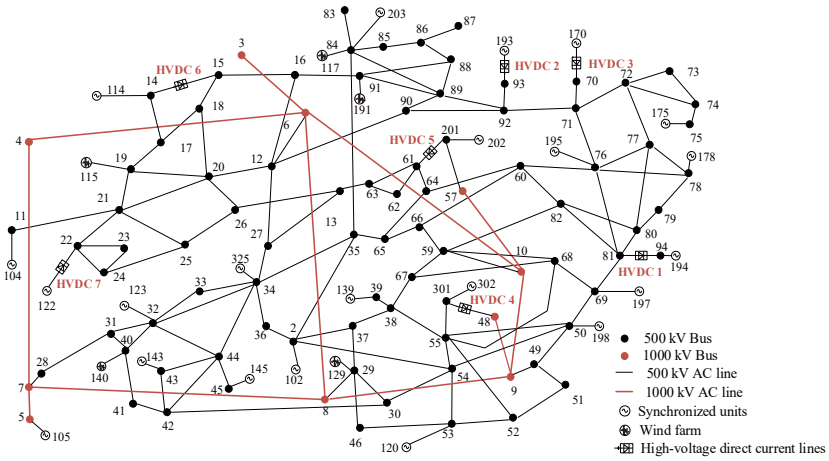


Figure 7. Topology of the receiving-end power system at Region C.

5.2. Verification of the Accuracy of the SFR Model of the VPP

Considering the randomness and diversity of faults, the fault scenarios are set as the operating conditions when a unipolar/bipolar blocking fault occurs in HVDC1-HVDC7 at 1 s, or when the load of the grid is perturbed according to the load increase of 0.1%, 0.2%, . . ., 9.9%, or 10.0% of the total load, or when the two types of faults are randomly combined.

(1) Different model orders

Set the simulation time to 20 s, the simulation step size to 0.01 s, and the number of iterations n = 0. The three models—the first-order model, the second-order model, and the third-order model—are used to estimate the parameters of the VPP feedback control branch (the cutoff errors ε_a and ε_b of the model parameters a_i and b_j are 0.01, respectively) and set the number of fault scenarios to 1000. In each fault scenario, the frequency minimum and QSSF obtained from the SFR modeling of the detailed feedback control branch counting the VPP are used as the real values. The initial values of the first-order model parameters are set as $a_{0,\mathrm{est}(0)}$ = 0.5, $a_{1,\mathrm{est}(0)}$ = 7.0, $b_{0,\mathrm{est}(0)}$= 15.0, and $b_{1,\mathrm{est}(0)}$ = 15.0.

As shown in Table 2, after the first iteration, the parameter estimates increase significantly, realizing one approximation to the optimal solution. After the second iteration, the parameter estimates continue to increase, but the increment decreases. Although the change of estimated parameters $a_{1,\mathrm{est}}$ $\Delta a_{1,\mathrm{est}}$ is smaller than the cutoff error ε_a at this time, the change of other parameters still does not satisfy the termination condition, so it is necessary to continue the calculation. After the third iteration, the change of each estimated parameter satisfies the cutoff error, and the optimization calculation is finished, and the results under the third iteration are recorded as the estimated parameters of the first-order model. Similarly, the solution process of second-order and third-order models conditional on increasing numbers of iterations are shown in Tables 3 and 4.

Table 2. Parameter changes of iterations under the first-order model.

Number of Iterations	$a_{0,est}$	$a_{1,est}$	$b_{0,est}$	$b_{1,est}$
0	0.500	7.000	15.000	15.000
1	0.863	8.995	15.827	32.320
2	0.991	9.002	16.136	38.881
3	0.998	9.007	16.142	38.889

Table 3. Parameter changes of iterations under the second-order model.

Number of Iterations	$a_{0,est}$	$a_{1,est}$	$a_{2,est}$	$b_{0,est}$	$b_{1,est}$
0	0.500	7.000	1.000	15.000	15.000
1	0.859	8.376	2.018	15.715	32.002
2	0.995	8.949	2.612	16.134	38.878
3	0.997	9.291	2.695	16.140	38.885
4	0.998	9.293	2.697	16.141	38.884

Table 4. Parameter changes of iterations under third-order model.

Number of Iterations	$a_{0,est}$	$a_{1,est}$	$a_{2,est}$	$a_{3,est}$	$b_{0,est}$	$b_{1,est}$
0	0.500	7.000	1.000	0.5	15.000	15.000
1	0.857	8.816	3.761	0.712	15.795	32.202
2	0.995	9.336	4.680	0.777	16.134	38.876
3	0.996	9.591	5.594	0.805	16.138	38.884
4	0.998	9.594	5.597	0.807	16.141	38.885
5	0.999	9.595	5.601	0.808	16.142	38.885

Equivalent feedback control branch model order affects the frequency response model accuracy. For the three model orders, the error between the estimated and true values of the lowest frequency and quasi-steady-state frequency is shown in Figure 8.

The absolute errors between the true and estimated values of the minimum frequency and QSSF are greater than zero in each of the predicted fault scenarios, which reflects conservativeness of the model. As the order of the model increases, the errors of the lowest value of frequency and the quasi-steady-state frequency become smaller. When the third-order model is used, the absolute errors of the frequency minimum and the QSSF are about less than 0.01 Hz and 0.005 Hz. Even if the first-order model is used, the error of the frequency minimum is less than 0.05 Hz, i.e., 0.001 p.u., and that of the QSSF is less than 0.015 Hz, i.e., 0.0003 p.u., which meets the requirements of engineering applications.

(2) The influence of different initial values

To analyze the impact of different initial values on parameter estimation, based on the first-order model, three sets of different initial values were set. The first set was consistent with the initial values in Table 2. The second set of initial values approached the lower limit of the parameters, $a_{0,est(0)} = 0.1$, $a_{1,est(0)} = 4.0$, $b_{0,est(0)} = 12.5$, and $b_{1,est(0)} = 5.0$. The initial value of the third group was set close to the upper limit of the parameter, $a_{0,est(0)} = 2.0$, $a_{1,est(0)} = 11.0$, $b_{0,est(0)} = 33.0$, and $b_{1,est(0)} = 100.0$. The remaining settings of the algorithm remain unchanged. The parameter estimation process under the second and third initial values is shown in Figure 9.

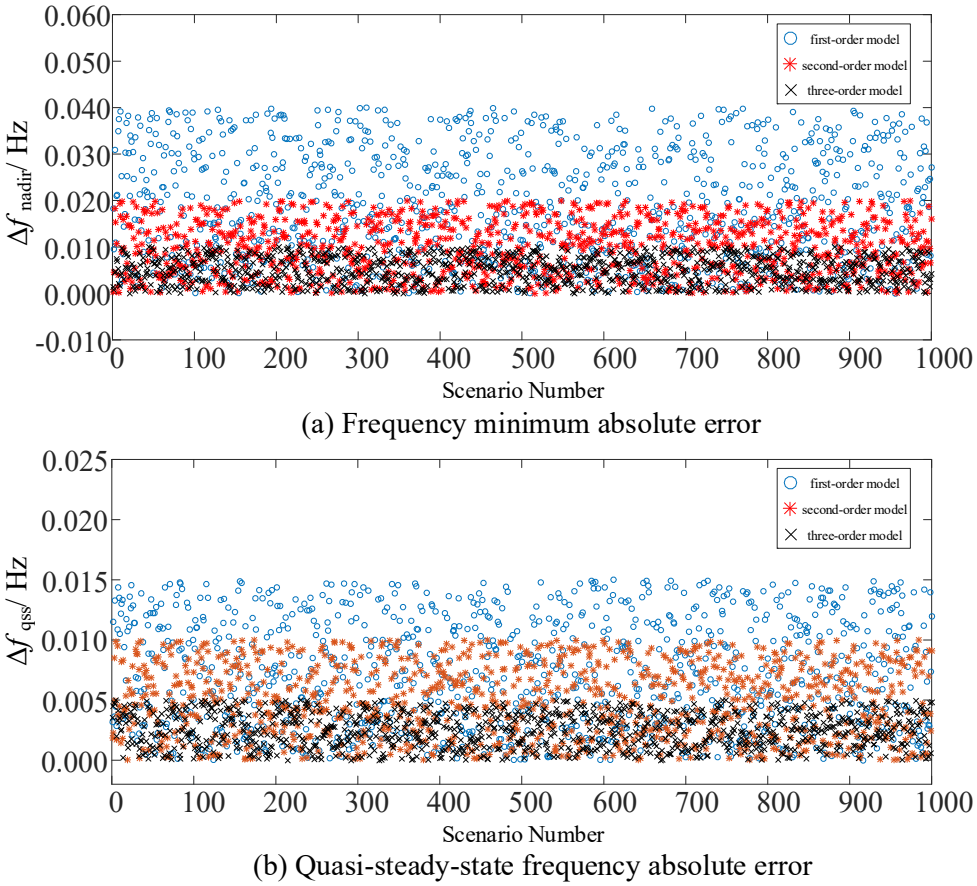


Figure 8. Absolute error of frequency nadir and quasi-steady-state frequency.

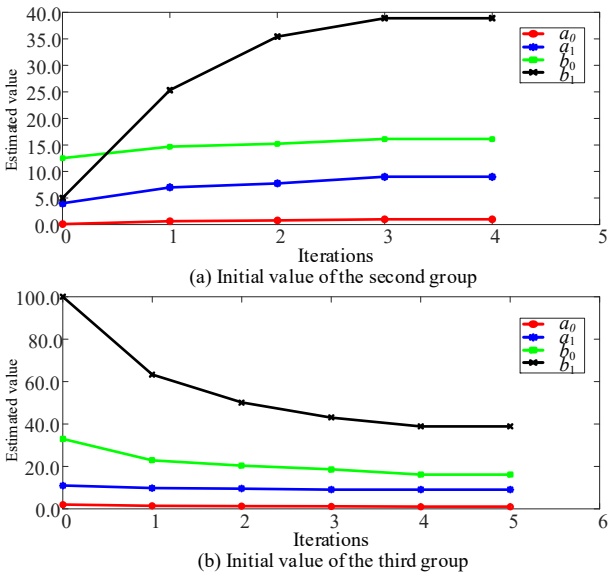


Figure 9. Parameter changes of iterations under different initial values.

According to the results in Figure 9, when setting different initial values for parameter estimation, the estimated values obtained through algorithm iteration are close. Based on the estimated parameters under the first set of initial values, the absolute error of the estimated values for the other two sets of parameters is in the order of 10^{-3}. Regardless of whether the initial value is set high or low, it can still approach the optimal solution

after solving, indicating that the parameter estimation optimization model proposed in this paper has good adaptability under different initial parameters.

(3) Comparative analysis

In this chapter, the proposed parameter estimation method is compared with the parameter estimation methods in time-domain simulation, least squares method, and Reference [19]. Among them, the third-order model with higher accuracy is used in the proposed method in this paper, and the initial values are set to be consistent with those in Table 4. The fitting function in the nonlinear least squares method adopts Equation (10) in Reference [25], which is an expression describing the relationship between the SFR and each control parameter. In Reference [19], the typical initial values are set to be T_R = 0.2 s, T_b = 0.3 s, T_{RH} = 7 s, and F_h = 0.3. The fault scenario is set as a precipitous increase in grid load of 700 MW at 1 s. The SFR curves under different methods are shown in Figure 10, and the frequency key indexes and errors are shown in Table 5.

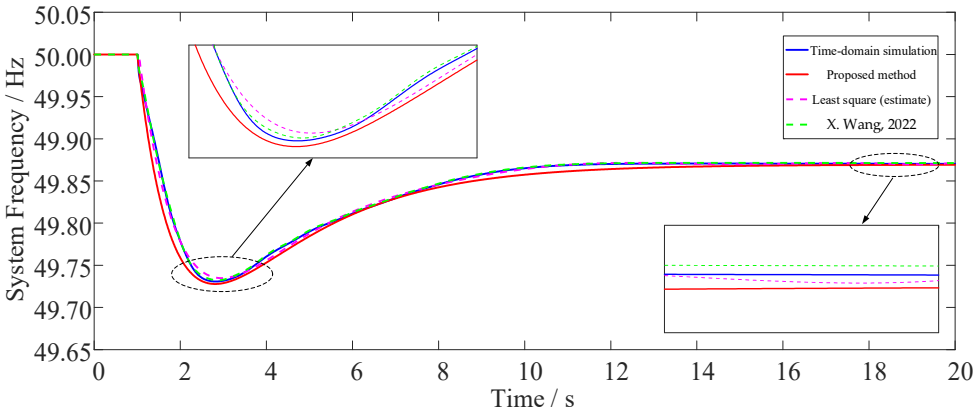


Figure 10. System frequency response curves under different methods [19].

Table 5. Frequency indices and relative errors under different methods.

Methodology	Minimum Frequency/Hz	Quasi-Stationary Frequency/Hz	Relative Error/%	
			Minimum Frequency	Quasi-Stationary Frequency
Time-domain simulation	49.7308	49.8704	-	-
Least square (estimate)	49.7347	49.8699	0.0078	0.0010
Reference [19]	49.7323	49.8712	0.0030	0.0016
Methodology of this paper	49.7278	49.8692	0.0060	0.0024

Due to the high computational accuracy of time-domain simulation, other methods often use it as a reference value for comparison. According to the results in Figure 10 and Table 5, the lowest point of the system frequency obtained using the nonlinear least squares method is higher than the calculated value of the time-domain simulation, with a relative error of 0.0078%, which is somewhat optimistic. Reference [19] constructed an optimization model with the objective of minimizing the sum of squares of the difference between the true and estimated frequency values, and solved it using optimization methods such as steepest descent and Newton's method to obtain the estimated parameters. This method has high computational accuracy and is suitable for analyzing the dynamic characteristics of system frequency response. However, it cannot guarantee the conservatism of key frequency indicators, that is, the lowest frequency value and quasi-steady-state frequency value of the system may be higher than the results of time-domain simulation, making it difficult to use for emergency frequency control optimization decision making. In addition, both of the above methods require a large amount of sampling of the system frequency after the fault to obtain the computational data required by the algorithm. However, the

method proposed in this paper can achieve good computational accuracy with simpler inputs, simpler implementation, and good accuracy. In this scenario, the relative error of the frequency index is in the order of 10^{-3}. And the method proposed in this article only needs to take the frequency key indicator values (the minimum frequency and quasi-steady-state frequency) as inputs. The frequency key indicator constraint of the optimization model stipulates that the frequency value obtained by the method in this article is lower than the time-domain simulation. This can reflect the conservatism of the method in this article and avoid missed judgments in emergency frequency control decisions.

6. Conclusions

VPP participates in emergency frequency control by aggregating multiple types of flexible resources, but it is difficult to construct the frequency response model of VPP because the SFR characteristics of each resource are different and the VPP model is characterized by complexity, high order, and unknown parameters. In this paper, the SLP algorithm is used to perform parameter estimation on VPP frequency response model considering multiple flexible resources, and the methodological innovations are as follows:

(1) The VPP frequency response model proposed in this paper takes into account the frequency response characteristics of various types of resources and analyzes the role of each control mode on frequency support based on the inertia response, primary frequency modulation, and fast power control in multiple dimensions.
(2) The SLP-based parameter estimation method for the VPP SFR model only needs to take the value of frequency key index as input, which is simple to implement and has high accuracy. In addition, the parameter estimation results are conservative, which can prevent the system from misjudging in the emergency frequency control decision.
(3) The scientific validity and soundness of the proposed methodology in this paper is verified by simulation through a multi-fault test scenario based on a three-region HVDC receiving area grid C. Even if a first-order model is used for parameter estimation, the error of its frequency key index is less than 0.001 p.u., which meets the requirements of engineering applications.

The method in this article is to aggregate distributed resources at a voltage level of 500 kV and construct a system frequency response model considering VPP, which can support emergency frequency control. This article analyzes and considers the frequency response model construction of VPP from the system level, so there is no more detailed modeling of various distributed resources at the device level, which is also the direction for our future improvement.

Author Contributions: All authors contributed to the research in the paper. Conceptualization, Z.S. and H.Z. (Haixiao Zhu); data curation, H.Z. (Haibo Zhao); formal analysis, P.W. and K.W.; funding acquisition, Y.L.; investigation, Z.S. and K.W.; methodology, H.Z. (Haibo Zhao) and J.C.; resources, X.Z.; software, Z.S. and H.L.; supervision, H.Z. (Haibo Zhao), P.W. and Y.L.; validation, Z.S.; visualization, J.C.; Writing—original draft, H.L.; writing—review and editing, Z.S. and H.Z. (Haixiao Zhu). All authors have read and agreed to the published version of the manuscript.

Funding: This research received no external funding.

Data Availability Statement: The original contributions presented in the study are included in the article, further inquiries can be directed to the corresponding author.

Conflicts of Interest: Authors Zheng Shi, Haibo Zhao, Peng Wang, Yan Liang, Kaikai Wang, Jie Chen, Xiaoming Zheng and Hongli Liu were employed by the Economic and Technical Research Institute of State Grid Shanxi Electric Power Company. The authors declare that the research was conducted in the absence of any commercial or financial relationships that could be construed as a potential conflict of interest.

References

1. Cui, R.Y.; Hultman, N.; Cui, D.; McJeon, H.; Yu, S.; Edwards, M.R.; Sen, A.; Song, K.; Bowman, C.; Clarke, L.; et al. A plant-by-plant strategy for high-ambition coal power phaseout in China. *Nat. Commun.* **2021**, *12*, 1468. [CrossRef] [PubMed]
2. Cao, Y.; Zhang, H.; Zhang, Y.; Li, C.G. Event-driven Fast Frequency Response Control Method for Generator Unit. *Autom. Electr. Power Syst.* **2021**, *45*, 148–154.
3. Chen, C.; Li, N.; Zhong, P.; Zeng, M. Review of Virtual Power Plant Technology Abroad and Enlightenment to China. *Power Syst. Technol.* **2013**, *37*, 2258–2263.
4. Hernandez, L.; Baladron, C.; Aguiar, J.M.; Carro, B.; Sanchez-Esguevillas, A.; Lloret, J.; Chinarro, D.; Gomez-Sanz, J.J.; Cook, D. A multi-agent system architecture for smart grid management and forecasting of energy demand in virtual power plants. *IEEE Commun. Mgz.* **2013**, *51*, 106–113. [CrossRef]
5. Wei, Z.; Yu, S.; Sun, G.; Sun, Y.; Yuan, Y.; Wang, D. Concept and Development of Virtual Power Plant. *Autom. Electr. Power Syst.* **2013**, *37*, 1–9.
6. Zhou, B.; Zhang, K.; Chan, K.W.; Li, C.; Lu, X.; Bu, S.; Gao, X. Optimal coordination of electric vehicles for virtual power plants with dynamic communication spectrum allocation. *IEEE Trans. Ind. Inform.* **2020**, *17*, 450–462. [CrossRef]
7. Chen, W.; Ai, X.; Fan, Y. Replicator Dynamics Algorithm Based Equilibrium Dispatching Strategy for Distributed Energy Resources in Virtual Power Plant. *Power Syst. Technol.* **2014**, *38*, 589–595.
8. Zhang, Y.; Mu, Y.; Jia, H.; Wang, M.; Zhou, Y.; Xu, Z. Response Capability Evaluation Model with Multiple Time Scales for Electric Vehicle Virtual Power Plant. *Autom. Electr. Power Syst.* **2019**, *43*, 94–103.
9. Lu, Z.; Wang, H.; Zhao, H.; Feng, H. Double layer inverse robust optimization scheduling strategy for virtual power plants containing V2G. *Power Syst. Technol.* **2017**, *41*, 1245–1252.
10. Xu, Q.; Cao, Y.; Zhang, H. Preventative Control Method for Virtual Power Plant Considering Transient Frequency Regulation Capability. *Autom. Electr. Power Syst.* **2022**, *46*, 83–89.
11. Li, R.; Xu, T.; Li, Y.; Zhang, E.; Cui, L. Study on primary frequency modulation characteristics of virtual power plant using different control strategies. *Mod. Electron. Tech.* **2021**, *44*, 95–99.
12. Wang, J.; Liao, S.; Yao, L.; Pu, T.; Xu, J.; Liu, Y.; Cheng, F. A Coordinated Frequency Control for HVDC Receiving-End Power Grid with Distributed Frequency Regulation Resources Based on Consensus Algorithm. *Power Syst. Technol.* **2022**, *46*, 888–900.
13. Wang, S.; Wu, W. Aggregate flexibility of virtual power plants with temporal coupling constraints. *IEEE Trans. Smart Grid* **2021**, *12*, 5043–5051. [CrossRef]
14. Jiang, Z.; Zhang, F.; Hu, F.; Sun, Y.; Jiang, W.; Deng, Y. Aggregation response capability evaluation method of distributed resources in virtual power plant. *Electr. Power Eng. Technol.* **2022**, *41*, 39–49.
15. Chen, J.; Liu, M.; Milano, F. Aggregated model of virtual power plants for transient frequency and voltage stability analysis. *IEEE Trans. Power Syst.* **2021**, *36*, 4366–4375. [CrossRef]
16. Feng, C.; Chen, Q.; Wang, Y.; Kong, P.-Y.; Gao, H.; Chen, S. Provision of Contingency Frequency Services for Virtual Power Plants with Aggregated Models. *IEEE Trans. Smart Grid* **2022**, *14*, 2798–2811. [CrossRef]
17. Inoue, T.; Taniguchi, H.; Ikeguchi, Y.; Yoshida, K. Estimation of power system inertia constant and capacity of spinning-reserve support generators using measured frequency transients. *IEEE Trans. Power Syst.* **1997**, *12*, 136–143. [CrossRef]
18. Liu, M.; Chen, J.; Milano, F. On-line inertia estimation for synchronous and non-synchronous devices. *IEEE Trans. Power Syst.* **2020**, *36*, 2693–2701. [CrossRef]
19. Wang, X.; Li, X.; Guo, L.; Zhao, Z.; Wang, H.; Wang, C. Parameter Estimation Method of a Frequency Response Model of Multi-Area Interconnected Power System Based on Cross-Section Information. *Power Syst. Technol.* **2022**, *46*, 4277–4291.
20. Han, S.; Xu, Z.; Wu, X.; Jin, X. Comparison of Mathematical Models for Transient Stability between PSD-BPA and PSS/E. *South Power Syst. Technol.* **2010**, *4*, 67–71.
21. Song, X.; Wu, X.C.; Liu, W.Z.; Xu, A.D.; Bu, G.Q.; Jing, X.M. New Quasi-Steady-State HVDC Models for PSD-BPA Power System Transient Stability Simulation Program. *Power Syst. Technol.* **2010**, *34*, 62–67.
22. Mauricio, J.M.; Marano, A.; Gomez-Exposito, A.; Ramos, J.L.M. Frequency regulation contribution through variable-speed wind energy conversion systems. *IEEE Trans. Power Syst.* **2009**, *24*, 173–180. [CrossRef]
23. Hui, H.; Ding, Y.; Chen, T.; Rahman, S.; Song, Y. Dynamic and Stability Analysis of the Power System With the Control Loop of Inverter Air Conditioners. *IEEE Trans. Ind. Electron.* **2021**, *68*, 2725–2736. [CrossRef]
24. Shi, Z.; Xu, Y.; Wang, Y.; He, J.; Li, G.; Liu, Z. Coordinating multiple resources for emergency frequency control in the energy receiving-end power system with HVDCs. *IEEE Trans. Power Syst.* **2023**, *38*, 4708–4723. [CrossRef]
25. Shi, Q.; Li, F.; Cui, H. Analytical method to aggregate multi-machine SFR model with applications in power system dynamic studies. *IEEE Trans. Power Syst.* **2018**, *33*, 6355–6367. [CrossRef]

Disclaimer/Publisher's Note: The statements, opinions and data contained in all publications are solely those of the individual author(s) and contributor(s) and not of MDPI and/or the editor(s). MDPI and/or the editor(s) disclaim responsibility for any injury to people or property resulting from any ideas, methods, instructions or products referred to in the content.